A graph theoretical approach for performance comparison of ICA for fMRI analysis

Qunfang Long[1], Suchita Bhinge[1], Yuri Levin-Schwartz[1], Vince D. Calhoun[2,3], Tülay Adalı[1]
Email: {qunfang1, adali}@umbc.edu
[1]Department of Computer Science and Electrical Engineering,
University of Maryland Baltimore County, Baltimore, MD 21250
[2]The Mind Research Network, Albuquerque, NM 87131
[3]Electrical and Computer Engineering Department,
University of New Mexico, Albuquerque, NM 87131

***Abstract*—Due to its relatively few assumptions, independent component analysis (ICA) has become a widely-used tool for the analysis of functional magnetic resonance imaging (fMRI) data. In its application, Infomax, has been by far the most frequently used ICA algorithm, primarily because it is the first ICA algorithm applied to fMRI analysis. However, now there are a number of more flexible ICA algorithms, which can exploit multiple types of statistical properties of the signals with fewer assumptions. In this work, we investigate the performance of Infomax and two of the more recent ICA algorithms, entropy bound minimization (EBM) and entropy rate bound minimization (ERBM), on resting state fMRI data derived from a large number of patients with schizophrenia (SZs) and healthy controls (HCs). In order to overcome the difficulty of directly comparing the performances of different ICA algorithms on real fMRI data, we propose the use of graph theoretic (GT) metrics to assess the quality of an ICA decomposition by measuring an algorithm's ability to capture the inherent differences between SZs and HCs. Our results show that ERBM, the algorithm which incorporates the greatest number of statistical properties of the signals, provides the best performance for fMRI analysis.**

I. Introduction

The use of blind source separation (BSS) for the analysis of functional magnetic resonance imaging (fMRI) data has facilitated the understanding of how different regions of the brain interact during the performance of a task and at rest. One of the most popular BSS techniques for the analysis of fMRI data is independent component analysis (ICA) [1]. ICA is able to extract latent sources from the observed data, through the assumption of statistical independence and a linear mixing model. Since the extracted components across different subjects are expected to share some similarity, BSS techniques such as group ICA (GICA) [2] have become popular for the analysis of multi-subject fMRI data.

Following the introduction of Infomax in 1995 [3], which has been useful for many applications, now there are a number of new ICA algorithms that have been developed, each incorporating different types of diversity—statistical property—of the sources, such as higher order statistics (HOS) and sample dependence [1], and in more flexible ways. Incorporating greater flexibility into the source model enables more accurate characterization of the latent sources, thus leading to improved performance of ICA algorithms that exploit multiple types of diversity over simpler models. However, for the analysis of fMRI data, to date, Infomax has been the most commonly used algorithm, most likely because it is the first ICA algorithm applied to fMRI analysis, provides reasonable results [4] and is the default ICA algorithm in toolboxes such as the group ICA of fMRI toolboxes such as the group ICA of fMRI toolbox (GIFT) [5]. Infomax has also been shown to show similar performance [6] to the popular FastICA algorithm [7]. Entropy bound minimization (EBM) [8] and entropy rate bound minimization (ERBM) [9] are two more recently introduced ICA algorithms and they have been shown to provide desirable performance on simulated and real fMRI data, see $e.g.$, [9], [10]. Despite their potential, there have been nearly no comparisons of the performance of Infomax, EBM and ERBM on real fMRI data, and those few studies that have looked at their relative performances, see $e.g.$, [6], [10], have used limited number of subjects and based the evaluation on subjective metrics. Due to the increasing number of large fMRI datasets that include hundreds and even thousands of subjects, applying these algorithms to larger datasets increases our confidence and promises to further elucidate the relative differences between these ICA algorithms.

The desire for such a comparison raises the issue of how to determine a metric for comparing the different ICA algorithms for real data. Algorithmic comparison for fMRI analysis is difficult as decompositions can be quite different depending on the modeling assumptions of the particular algorithm, and as such, matching of all the estimated components is usually not possible. This motivates the use of global measures, such as functional clustering using dendrograms [11], [12] and time course frequency power ratio [13], [14]. However, these metrics are slightly subjective, thus motivating the development of fully objective measures of algorithmic performance.

Graph theoretical (GT) analysis has become an efficient tool for studying the heterogeneity between different groups of subjects, such as patients with schizophrenia (SZs) and healthy controls (HCs) [15]. Typically, graphs are constructed from the anatomically or functionally defined brain components by using the components as nodes and their dependence such as temporal correlation or spatial mutual information (MI) as the edges [15]. Based on these graphs, certain metrics between components, such as centrality or small worldness [16], are

This work was supported in part by NSF 1631838 and NIH R01 EB 020407

used to quantify each component's importance for information transfer in functional brain networks or the overall efficiency of information transfer. Metrics are calculated for each subject, and used to capture variability of either individual subjects or of subjects groups [17]. We show that GT metrics can provide an efficient means of performing algorithmic comparison as well by evaluating each algorithm's ability to capture group differences.

In this study, we investigate the performance of Infomax, EBM and ERBM on a relatively large dataset, which contains fMRI data drawn from 88 SZs and 91 HCs using the GICA framework. In order to provide an efficient comparison of the performances of different algorithms, we use two global metrics, the dendrogram and time course frequency power ratio. We also propose the use of the GT metric—centrality—to evaluate the ability of each ICA algorithm to capture the latent differences between SZs and HCs. The results show that ERBM performs best in capturing the latent differences between two groups, suggesting that incorporating a greater number of statistical properties of the signals results in better performance.

II. Methods and materials

A. GICA

The GICA framework enables analysis of fMRI data from multiple subjects. Let the observed fMRI data from the kth subject be denoted by $\tilde{\mathbf{X}}^{[k]} \in \mathbb{R}^{T\times V}$, $1 \leq k \leq K$, where T denotes the number of time points and V denotes the number of voxels. To reduce the contamination from noise, principal component analysis (PCA), using an order suggested by the entropy rate based order selection technique described in [18], is employed to reduce the dimension of the data for each subject. For each subject, $\tilde{\mathbf{X}}^{[k]}$ is reduced in dimension from T to T', $\mathbf{X}^{[k]} = \mathbf{F}^{[k]}\tilde{\mathbf{X}}^{[k]}$, where $\mathbf{F}^{[k]} \in \mathbb{R}^{T'\times T}$ is the subject level reduction matrix, and the reduced data is $\mathbf{X}^{[k]} \in \mathbb{R}^{T'\times V}$. It is assumed that the subjects share a common component subspace, and the datasets are temporally concatenated to form a single data matrix $\tilde{\mathbf{Y}} \in \mathbb{R}^{KT'\times V}$, which is then reduced to $\mathbf{Y} \in \mathbb{R}^{N\times V}$ by a group level PCA, $\mathbf{Y} = \mathbf{G}\tilde{\mathbf{Y}}$, with $\mathbf{G} \in \mathbb{R}^{N\times KT'}$ as the group level reduction matrix and N as the order for the common observation subspace. Group components $\mathbf{S} \in \mathbb{R}^{N\times V}$ are then estimated by performing ICA on the common group subspace $\mathbf{Y}$:

$$\mathbf{Y} = \mathbf{AS}$$

where $\mathbf{A} \in \mathbb{R}^{N\times N}$ is the mixing matrix. ICA seeks to find a group demixing matrix $\mathbf{W}$ such that $\mathbf{W} = \mathbf{A}^{-1}$ and the estimated sources are $\hat{\mathbf{S}} = \mathbf{WY}$. The use of a single ICA on the common subspace of all datasets helps to preserve the order of the components across subjects. Following the completion of ICA, back-reconstruction is performed on $\hat{\mathbf{S}}$ to generate the corresponding subject-specific source estimates $\hat{\mathbf{S}}^{[k]} \in \mathbb{R}^{N\times V}$. In order to back-reconstruct $\hat{\mathbf{S}}^{[k]}$, the group level reduction matrix $\mathbf{G}$ is blocked by columns, $\mathbf{G} = [\mathbf{G}^{[1]}, \mathbf{G}^{[2]}, \cdots, \mathbf{G}^{[K]}]$ with $\mathbf{G}^{[k]} \in \mathbb{R}^{N\times T'}$. Then, $\hat{\mathbf{S}}^{[k]}$ are reconstructed by $\hat{\mathbf{S}}^{[k]} = \mathbf{WG}^{[k]}\mathbf{F}^{[k]}\tilde{\mathbf{X}}^{[k]}$, and the corresponding subject-specific time courses $\hat{\mathbf{A}}^{[k]} \in \mathbb{R}^{T\times N}$ are also reconstructed, $\hat{\mathbf{A}}^{[k]} = (\mathbf{F}^{[k]})^{\dagger}(\mathbf{G}^{[k]})^{\dagger}\mathbf{W}^{-1}$, where † represents the pseudoinverse.

The differences in separation performance for separate ICA algorithms, such as Infomax, EBM and ERBM, are related to differences in their assumed latent source models. Infomax is an ICA algorithm that takes only the diversity of non-Gaussianity into consideration using a distribution model implied by a fixed sigmoidal nonlinearity [3]. This fixed nonlinearity is a good match for very focal regions of activation, however it might significantly bias latent sources relating to broad regions, such as the default mode network [19]. In contrast to Infomax, EBM does not assume one specific distribution for the latent sources but instead attempts to upper bound their entropy through the use of several measuring functions. Each of these functions provides bounds on the entropy, with the tightest bound being closest to the true entropy. The use of these measuring functions makes it possible to match a wide variety of distributions, including those that are sub-Gaussian, super-Gaussian, unimodal, bimodal, symmetric, as well as skewed [8], thus potentially leading to more accurate estimation of the latent sources. Instead of bounding the entropy of latent sources, ERBM attempts to bound their entropy rate using measuring functions. By calculating the entropy rate of sources, one more type of diversity, namely, sample dependence, is taken into consideration. Since EBM and ERBM relax the assumptions placed on the fMRI sources by assuming flexible source distributions, they are expected to provide improved performance over Infomax. Additionally, ERBM is expected to have superior performance over the other two algorithms, since it matches the underlying properties of the fMRI components namely voxel-wise dependence and HOS.

B. Global analysis

To compare the performance of the three ICA algorithms, proper measures are needed. Since it can be difficult to exactly match all of the estimated components across different algorithms, it is hard to directly compare algorithmic performance on fMRI data. In order to resolve this issue, we propose the use of two global measures to compare the performances of ICA algorithms on real data.

1) Dendrogram: Though ICA assumes that the latent sources are fully independent, following the performance of ICA the extracted independent components (ICs) generally have some dependence due to their functional relevance. A dendrogram is a natural way to capture this relevance and facilitate interpretation of the results [20]. Hence, we propose the use of the dendrogram for the comparison of ICA algorithms. In this implementation, a dendrogram is generated using a hierarchical clustering algorithm based on the average distance between ICs within each cluster. The distance, D, between each pair of ICs is measured using the normalized mutual information (NMI), I_{norm}, and is defined as,

$$\begin{aligned} D(\hat{s}_1, \hat{s}_2) &= 1 - I_{\text{norm}}(\hat{s}_1, \hat{s}_2) \\ &= 1 - \frac{2I(\hat{s}_1, \hat{s}_2)}{I(\hat{s}_1, \hat{s}_1) + I(\hat{s}_2, \hat{s}_2)} \end{aligned}$$

where $I(\hat{s}_1, \hat{s}_2)$ is the mutual information between two estimated components $\hat{s}_1$ and $\hat{s}_2$. Hence, for two similar sources the distance between them would be close to 0 and for dissimilar sources it would be close to 1.

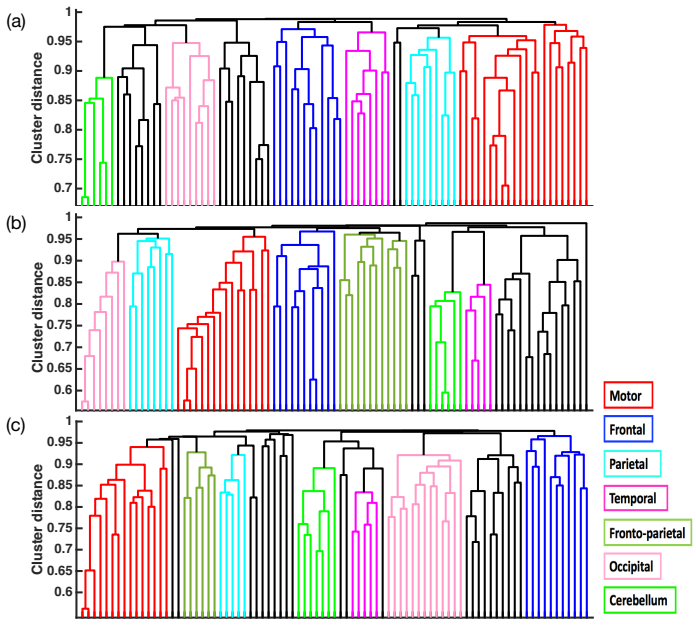

Fig. 1. Dendrograms of (a) Infomax (b) EBM (c) ERBM. Within each graph, the vertical lines are ICs and their length indicates the value of distance between each IC and its neighbors.

2) Frequency analysis: Another global measure of ICA algorithmic performance on real fMRI data is the ratio of time course power spectra in low-frequency band (< 0.1Hz) to the high-frequency band (> 0.15 Hz) for each IC. Since the activation in the components is due to the blood oxygen level-dependent (BOLD) response, which corresponds to the low frequencies, the lower the ratio between the low-frequency band and the high-frequency band, the more likely the component is to be describing cardiac or respiratory noise as opposed to true BOLD activation [13], [21].

C. Graph theoretical analysis

Though the previous two measures can be used to assess the performance of ICA algorithms on real fMRI data, they are slightly subjective. This motivates the use of objective GT metrics for assessing the performance of ICA algorithms. Prior to the construction of a given graph, for each algorithm and subject, N ICs are estimated and M components are selected based on their time course power ratio and visual inspection. Then, using the M ICs of interest as nodes and the NMI between the corresponding components as the edges, a fully connected graph, G, is constructed. Beginning with G, a percentage threshold, θ, is used to retain only the highest P percent of the edges, thus generating a new graph G$'$. We define the percentage of the edges that remain after thresholding as link density, which increases as the threshold increases. Then, the weighted graphs are converted to binary ones, with the edges below the threshold having a value of 0 and those above having a value of 1. In order to avoid very sparse graphs with small link densities and those with too large link densities, we limit the link density to range from 20% to 70%. We then perform a GT analysis on these graphs to

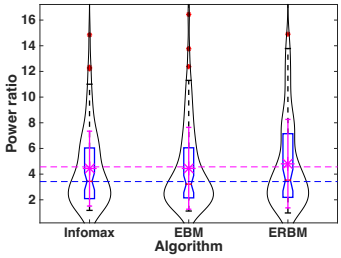

Fig. 2. Variances of the time course power ratio for three algorithms. The mean and stand deviation are in magenta, along with a box plot and smoothed density histogram.

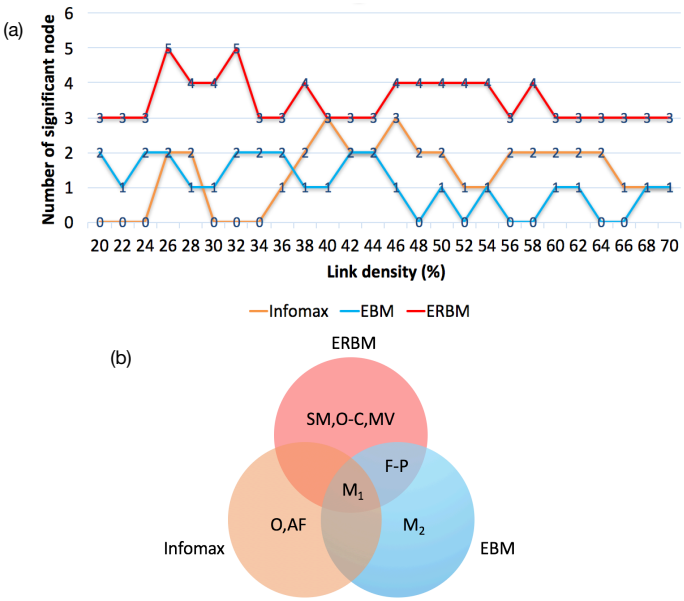

Fig. 3. (a) Number of nodes showing significant group difference in each graph as a function of link density. (b) The corresponding functional network for those nodes that show significant group differences. SM, sensorimotor; F-P, fronto-parietal; M, motor; O-C, occipital-cerebellum; MV, medial visual; P, parietal; S, sensory; DMN, default mode network; O, occipital; AF, anterior frontal.

calculate the centrality of each node:

$$H_i = \sum_{p \neq q \neq i}^{M} \frac{E_{p,i,q}}{E_{p,q}}$$

where $E_{p,i,q}$ is the number of shortest paths between pairwise nodes p and q that include node i, $E_{p,q}$ is the total number of shortest paths between nodes p and q. Note that high centrality of the ith node suggests that the ith IC is important in terms of the efficiency of the brain's functional network connectivity.

D. COBRE data

We use the resting state data of the COBRE dataset, which is available on the COINS data exchange repository (http://coins.mrn.org/dx) [22], as the fMRI data in this study. The resting state data includes 88 SZs (average age: 37 ± 14) and 91 HCs (average age: 38 ± 12). All images were collected on a single 3-Tesla Siemens Trio scanner with a 12-channel radio frequency coil using the following parameters: TE = 29

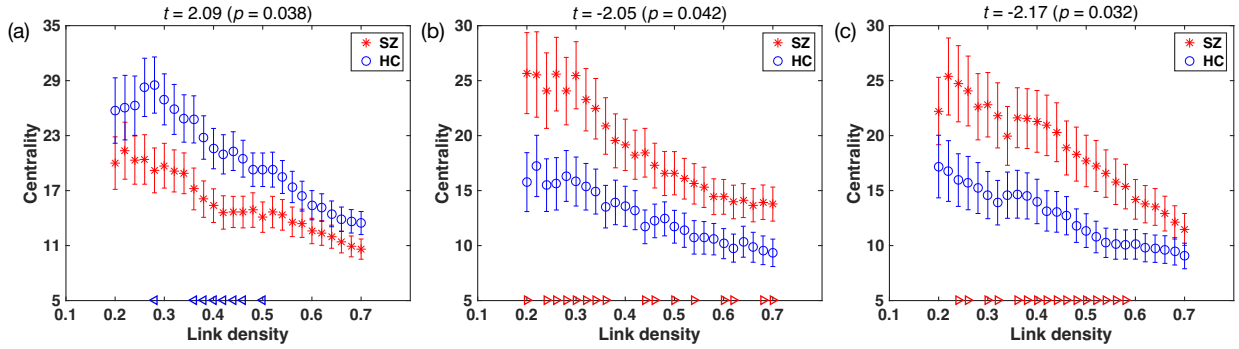

Fig. 4. Centrality plots for the motor component from (a) Infomax, (b) EBM and (c) ERBM. Red (blue) triangles along the x-axis indicate significantly higher (lower) centrality for the SZs group compared to HCs group. The average t-statistic in the region where the difference between the two groups is significant (0.28-0.5) for Infomax is $t = 2.09$ ($p = 0.038$), (0.2-0.5) for EBM is $t = -2.05$ ($p = 0.042$) and (0.24-0.58) for ERBM is $t = -2.17$ ($p = 0.032$).

ms, TR = 2 s, flip angle = 75°, slice thickness = 3.5 mm, slice gap = 1.05 mm, voxel size $3.75 \times 3.75 \times 4.55$ mm^3. Participants were instructed to keep their eyes open during the scan and stare passively at a central fixation cross. Each resting state scan is consisted of 150 volumes. The fMRI data were realigned with INRIalign algorithm [23], slice-timing correction was applied using the middle slice as the reference frame in the functional data pipeline and spatially normalized to the standard Montreal Neurological Institute space and resampled to $3 \times 3 \times 3$ mm^3, resulting in $53 \times 63 \times 46$ voxels. Then, the fMRI data are smoothed using a Gaussian kernel with a full-width at half-maximum of 10 mm.

III. Experimental Results

Accurate estimation of the number of common signals, N, is vital to the success of any application of an ICA algorithm. However, for fMRI data, classical order estimation techniques based on information theoretic criteria (ITC) may overestimate the order due to the inherent sample dependence of fMRI data [24], [25]. A common way to overcome this issue is by using downsampling to obtain effectively independent and identically distributed samples [24], [25]. Unfortunately, methods based on downsampling suffer from a loss of information associated with the downsampling. More recently, two entropy rate (ER)-based order estimation techniques are proposed that account for sample dependence without the use of downsampling: ER using a finite memory length model (ER-FM) and ER using an autoregressive model (ER-AR) [18]. Applying these two methods to each subject in the COBRE data separately, we find that the mean and standard deviation of the order across subjects are 72.86 ± 10.40 for ER-FM and 77.33 ± 10.91 for ER-AR. Since the sample correlation structure in ER-FM is a better match to that in fMRI data due to the finite span of correlation in the point spread function, we use an order equal to the mean plus one standard deviation estimated using ER-FM, which is rounded up to 85 to retain a significant level of the signal across multiple subjects while introducing minimal noise to some of the subjects. The use of this high model order is also well motivated in the literature for achieving a more useful functional segmentation of the brain, see *e.g.*, [13], [26].

The most stable run is selected using minimum spanning tree (MST) [19] method for EBM from 10 runs and for ERBM from 25 runs. Using back-reconstruction, the 85 ICs are estimated for individual subject associated with their time courses. All the analyses are performed on the back-reconstructed ICs and time courses.

A. Global comparison

Eighty-five mean ICs are generated by averaging the back-reconstructed ICs across all subjects. A dendrogram of the 85 mean ICs is plotted for each algorithm in Fig. 1. In Fig. 1, we label the different clusters using individual colors. The black lines indicate the ICs corresponding to ventricle, nuclei, thalamus, motion artifacts and a few incorrectly clustered ICs of interest. The dendrograms suggest that EBM and ERBM give clear clusters for all regions of interest, due to the fact that they provide a close match to the statistical properties of the data in their implementation. On the other hand, the results from Infomax do not give a clear fronto-parietal cluster, which is the main attention associated network in complex brain connectivity and of high interest in resting state fMRI data analysis [13]. Visual inspection of the ICs from Infomax indicates that there is no pure fronto-parietal component. There are three ICs containing the fronto-parietal network but have interference with motor. For this reason, Infomax identifies a very large motor cluster, since some frontal and parietal components are grouped into motor cluster.

The time course power ratio comparison among the three algorithms is shown in a violin plot in Fig. 2. The black curve is the smoothed distribution of ratio within all subjects. The blue box plot displays the median, the 25th and 75th percentiles of the time course power ratio with whiskers extending to the 99.3% confidence interval and some outliers beyond whisker. The mean and standard deviation are in magenta. Horizontal magenta and blue line refers to the global average, 4.57, and median power ratio, 3.42, across ICs from all three algorithms, respectively. From Fig. 2, we can see that ERBM has both the highest mean and median power ratio, though the difference is slightly hard to discern. This implies that the overall ICs estimated by ERBM correspond more closely to the BOLD response than those estimated by EBM and Infomax.

B. Graph theoretical analysis

The first step in constructing a graph for the estimated ICs consists of first selecting the ICs with time course power ratio

higher than 3. Then, through visual inspection the selected ICs with large edge effects and ventricles are removed. Finally, 37 components of interest for Infomax, 33 for EBM and 39 for ERBM are retained. The slight difference in number of retained components is due to the inherent differences among the three algorithms. The graph, G, is formed, where the retained components are nodes and pairwise NMI forms the edges.

For each binarized graph, the centrality is calculated for each node. We then perform a two-sample t-test on the centrality values of the SZs and HCs for each node, with an FDR corrected level of significance set at $p < 0.05$. In order to prevent nodes from being declared significant by chance, only those nodes that show significant differences in at least three successive graphs are declared to be truly significant. Fig. 3(a) shows the plot for the number of significant components at each link density. As can be seen in Fig. 3(a), each algorithm detects a different number of significant components. We can see that more components from ERBM show consistent significance in graphs for the majority of link density values, which gives us a greater ability to explore the differences between the two groups. Fig. 3(b) shows the corresponding brain areas of each significant component. We note that all three algorithms have at least one motor component that shows a significant group difference. Finally, note that EBM and ERBM have fronto-parietal components that show significant difference while Infomax does not.

The results of the GT analysis of the centrality of the motor component, which is the only common component that shows consistent significant group difference for each algorithm, are shown in Fig. 4. From Fig. 4, it is clear that as link density increases, the centrality of motor component for each method decreases. The motor component from EBM and ERBM shows significantly higher centrality in SZs compared to HCs, while that from Infomax shows lower centrality in SZs compared to HCs. A potential reason for the fact that the motor component from Infomax, unlike those from EBM and ERBM, shows significantly higher centrality for HCs is because this motor component is unilateral but those of EBM and ERBM are bilateral. In order to ensure that the differences between the groups are not purely coincidental, we seek differences that are consistent across a range of link densities. For this reason, we measure the consistency of the differences across subjects in two ways: first, in terms of the total range of density values for which we see statistically significant differences, and second, in terms of the average statistical difference between the groups observed throughout this "significance interval." The interval of graph link density in which the motor component shows significant difference is 0.22 for Infomax, 0.5 for EBM and 0.34 for ERBM. This means that by using EBM, we observe the highest stability of the statistical differences across link density values of all the applied ICA algorithms. The averaged t-statistic from two-sample t-test in corresponding significant interval is $t = 2.09$ $(p = 0.038)$ for Infomax, $t = -2.05$ $(p = 0.042)$ for EBM, $t = -2.17$ $(p = 0.032)$ for ERBM. It indicates that the motor components from ERBM show greater significance in its significant interval.

IV. Conclusion

The use of BSS methods, such as GICA, for the analysis of multi-subject fMRI data enables us to uncover the structural disruptions inherent to patients affected by neurodegenerative diseases. However, the strength of these claims is based on the power of the ICA algorithm used to obtain the results. In this paper, we investigate the performance of GICA using three ICA algorithms, namely, Infomax, EBM and ERBM, on a large fMRI dataset. In order to compare the performances of different ICA algorithms on real fMRI data, we propose the use of global measures to compare the overall usefulness of the ICs generated by each algorithm. We also use GT metrics to evaluate the performance of ICA algorithms by comparing their ability to capture differences between patients with schizophrenia and healthy controls. Our experimental results suggest that ERBM gives the best performance, which implies that incorporating more statistical information contributes to the extraction of more meaningful components. We also note that GT analysis is a promising method to assess the performance of ICA algorithms on fMRI data drawn from multiple groups, thus motivating the use of GT metrics to assess algorithmic performance for other neuroscience studies.

References

[1] T. Adalı, M. Anderson, and G.-S. Fu, "Diversity in independent component and vector analyses: Identifiability, algorithms, and applications in medical imaging," *IEEE Signal Processing Magazine*, vol. 31, no. 3, pp. 18–33, May 2014.

[2] V. D. Calhoun, T. Adalı, G. D. Pearlson, and J. J. Pekar, "A method for making group inferences from functional MRI data using independent component analysis," *Human Brain Mapping*, vol. 14, no. 3, pp. 140–151, 2001.

[3] A. Bell and T. Sejnowski, "An information maximization approach to blind separation and blind deconvolution," *Neural Computation*, vol. 7, pp. 1129–1159, 1995.

[4] M. J. Mckeown, S. Makeig, G. G. Brown, T.-P. Jung, S. S. Kindermann, A. J. Bell, and T. J. Sejnowski, "Analysis of fMRI Data by Blind Separation Into Independent Spatial Components," *Human Brain Mapping*, vol. 6, pp. 160–188, 1998.

[5] GIFT, "Group ICA of fMRI Toolbox (GIFT)," http://mialab.mrn.org/software/gift/index.html, 2011.

[6] N. Correa, T. Adalı, and V. D. Calhoun, "Performance of blind source separation algorithms for fMRI analysis using a group ica method," *Magnetic Resonance Imaging*, vol. 25, no. 5, pp. 684–694, 2007.

[7] A. Hyvärinen and E. Oja, "A fast fixed-point algorithm for independent component analysis," *Neural computation*, vol. 9, no. 7, pp. 1483–1492, 1997.

[8] X.-L. Li and T. Adalı, "Independent component analysis by entropy bound minimization," *IEEE Transactions on Signal Processing*, vol. 58, no. 10, pp. 5151–5164, Dec. 2010.

[9] ——, "Blind spatiotemporal separation of second and/or higher-order correlated sources by entropy rate minimization," in *2010 IEEE International Conference on Acoustics Speech and Signal Processing (ICASSP)*, March 2010, pp. 1934–1937.

[10] W. Du, H. Li, X.-L. Li, V. D. Calhoun, and T. Adalı, "ICA of fMRI data: Performance of three ICA algorithms and the importance of taking correlation information into account," in *2011 IEEE International Symposium on Biomedical Imaging: From Nano to Macro*, April 2011, pp. 1573 –1576.

[11] D. Cordes, V. Haughton, J. D. Carew, K. Arfanakis, and K. Maravilla, "Hierarchical clustering to measure connectivity in fMRI resting-state data," *Magnetic Resonance Imaging*, vol. 20, no. 4, pp. 305–317, 2002.

[12] S. M. Smith, C. F. Beckmann, J. Andersson, E. J. Auerbach, J. Bijsterbosch, G. Douaud, E. Duff, D. A. Feinberg, L. Griffanti, M. P. Harms *et al.*, "Resting-state fMRI in the human connectome project," *Neuroimage*, vol. 80, pp. 144–168, 2013.

[13] E. A. Allen, E. B. Erhardt, E. Damaraju, W. Gruner, J. M. Segall, R. F. Silva, M. Havlicek, S. Rachakonda, J. Fries, R. Kalyanam *et al.*, "A baseline for the multivariate comparison of resting-state networks," *Front. Syst. Neurosci.*, vol. 5, p. 2, 2011.

[14] S. Robinson, G. Basso, N. Soldati, U. Sailer, J. Jovicich, L. Bruzzone, I. Kryspin-Exner, H. Bauer, and E. Moser, "A resting state network in the motor control circuit of the basal ganglia," *BMC Neuroscience*, vol. 10, no. 1, p. 1, 2009.

[15] E. Bullmore and O. Sporns, "Complex brain networks: graph theoretical analysis of structural and functional systems," *Nature Reviews Neuroscience*, vol. 10, no. 3, pp. 186–198, 2009.

[16] M. Rubinov and O. Sporns, "Complex network measures of brain connectivity: uses and interpretations," *NeuroImage*, vol. 52, no. 3, pp. 1059–1069, 2010.

[17] J. Laney, K. P. Westlake, S. Ma, E. Woytowicz, V. D. Calhoun, and T. Adalı, "Capturing subject variability in fMRI data: A graph-theoretical analysis of GICA vs. IVA," *Journal of Neuroscience Methods*, vol. 247, pp. 32–40, 2015.

[18] G.-S. Fu, M. Anderson, and T. Adalı, "Likelihood estimators for dependent samples and their application to order detection," *IEEE Transactions on Signal Processing*, vol. 62, no. 16, pp. 4237–4244, Aug. 2014.

[19] W. Du, Y. Levin-Schwartz, G.-S. Fu, S. Ma, V. D. Calhoun, and T. Adalı, "The role of diversity in complex ICA algorithms for fMRI analysis," *Journal of Neuroscience Methods*, vol. 264, pp. 129–135, 2016.

[20] S. Ma, N. Correa, X.-L. Li, T. Eichele, V. D. Calhoun, and T. Adalı, "Automatic identification of functional clusters in fMRI data using spatial dependence," *IEEE Transactions on Biomedical Engineering*, vol. 58, no. 12, pp. 3406–3417, 2011.

[21] D. Cordes, V. M. Haughton, K. Arfanakis, J. D. Carew, P. A. Turski, C. H. Moritz, M. A. Quigley, and M. E. Meyerand, "Frequencies contributing to functional connectivity in the cerebral cortex in resting-state data," *American Journal of Neuroradiology*, vol. 22, no. 7, pp. 1326–1333, 2001.

[22] A. Scott, W. Courtney, D. Wood, R. De la Garza, S. Lane, R. Wang, M. King, J. Roberts, J. A. Turner, and V. D. Calhoun, "COINS: an innovative informatics and neuroimaging tool suite built for large heterogeneous datasets," *Frontiers in Neuroinformatics*, vol. 5, p. 33, 2011.

[23] L. Freire, A. Roche, and J.-F. Mangin, "What is the best similarity measure for motion correction in fMRI time series?" *IEEE Transactions on Medical Imaging*, vol. 21, no. 5, pp. 470–484, 2002.

[24] Y.-O. Li, T. Adalı, and V. D. Calhoun, "Estimating the number of independent components for functional magnetic resonance imaging data," *Human Brain Mapping*, vol. 28, no. 11, pp. 1251–1266, 2007.

[25] X.-L. Li, S. Ma, V. D. Calhoun, and T. Adalı, "Order detection for fMRI analysis: Joint estimation of downsampling depth and order by information theoretic criteria," in *IEEE Int. Symp. Biomedical Imaging: From Nano to Macro*, April 2011, pp. 1019–1022.

[26] V. Kiviniemi, T. Starck, J. Remes, X. Long, J. Nikkinen, M. Haapea, J. Veijola, I. Moilanen, M. Isohanni, Y.-F. Zang *et al.*, "Functional segmentation of the brain cortex using high model order group PICA," *Human Brain Mapping*, vol. 30, no. 12, pp. 3865–3886, 2009.